Aerotecnica Missili & Spazio
https://doi.org/10.1007/s42496-024-00208-6

ORIGINAL ARTICLE

Development of a Ferrofluid-Based Attitude Control Actuator for Verification on the ISS

Sebastian Zajonz[1] · Christian Korn[1] · Steffen Großmann[1] · Janoah Dietrich[1] · Maximilian Kob[1] · Daniel Philipp[1] · Fabrizio Turco[1] · Michael Steinert[1] · Michael O'Donohue[1] · Nicolas Heinz[1] · Elizabeth Gutierrez[1] · Alexander Wagner[1] · Daniel Bölke[1] · Saskia Sütterlin[1] · Maximilian Schneider[1] · Yolantha Remane[1] · Phil Kreul[1] · Bianca Wank[1] · Manuel Buchfink[1] · Denis Acker[1] · Sonja Hofmann[1] · Bahar Karahan[1] · Silas Ruffner[1] · Manfred Ehresmann[2] · Felix Schäfer[2] · Georg Herdrich[2]

Received: 23 October 2023 / Revised: 11 February 2024 / Accepted: 12 February 2024

Abstract

Ferrofluid-based systems provide an opportunity for increasing the durability and reliability of systems, where mechanical parts are prone to wear and tear. Conventional reaction control systems are based on mechanically mounted rotating disks. Due to inherent friction, they suffer from degradation, which may eventually lead to failure. This problem is further intensified due to the limited possibility for repair and maintenance. Ferrofluid-based systems aim to replace mechanical components by exploiting ferrofluidic suspended motion. Ferrofluids consist of magnetic nanoparticles suspended in a carrier fluid and can be manipulated by external magnetic fields. This paper describes the working principle, design, and integration of a working prototype of a ferrofluid-based attitude control system (ACS), called Ferrowheel. It is based on a stator of a brushless DC motor in combination with a rotor on a ferrofluidic bearing. The prototype will be verified in a microgravity environment on the International Space Station, as part of the Überflieger 2 student competition of the German Aerospace Center. First ground tests deliver positive results and confirm the practicability of such a system.

Keywords FARGO · ISS · DLR · Ferrofluid · ACS · Student Project · Wear-reduction · Mechanic-free

List of Symbols

I	Moment of Inertia [kg·m^2]
L	Angular Momentum [Nms]
p	Momentum [Nm]
r	Distance [m]
t	Time [s]
T	Torque [Nm]
U	Voltage [V]
I_A	Current [A]
ϕ	Angle [rad]
ω	Angular Velocity [$\frac{\text{rad}}{s}$]
$\dot{\omega}, \alpha$	Angular Acceleration [$\frac{\text{rad}}{s^2}$]

Abbreviations

ACS	Attitude Control Systems
AOCS	Attitude and Orbit Control System
BLDC	Brushless Direct Current (Motor)
COTS	Commercial of the Shelf
DC	Direct Current
DLR	German Aerospace Center
DPG	German Physical Society
ESA	European Space Agency
ESC	Electronic Speed Controller
FARGO	Ferrofluid Application Research Goes Orbital
IR	Infra-Red
IRS	Institute of Space Systems, University of Stuttgart
ISS	International Space Station
KSat	Small Satellite Student Association, University of Stuttgart

Sebastian Zajonz and Christian Korn have contributed equally to this work.

✉ Georg Herdrich
herdrich@irs.uni-stuttgart.de

Sebastian Zajonz
sebastian.zajonz@ksat-stuttgart.de

Christian Korn
korn@ksat-stuttgart.de

[1] KSat e.V., Pfaffenwaldring 29, 70569 Stuttgart, Germany

[2] Institute of Space Systems University of Stuttgart, Pfaffenwaldring 29, 70569 Stuttgart, Germany

Published online: 26 April 2024

MoI	Moment of Inertia
PAPELL	Pump Application using Pulsed Electromagnets for Liquid reLocation
PC	Polycarbonate
PTFE	Polytetrafluorethylen
RPM	Revolutions per Minute
RW	Reaction Wheel

1 Introduction

In space applications, maintenance is either impossible or difficult, and development expenses of mechanical systems are high. The durability and reliability of each component is critical to mission success. Additionally, moving parts have the drawback of being prone to wear and tear while having inherent friction, often necessitating an inevitable need for maintenance. Thus, mechanical parts have a finite lifespan and are prone to failure. Surfaces in direct mechanical contact will inevitably deteriorate. This leads to a hard trade-off between very resource-consuming reparations or forfeiting the lifetime of the components and accepting mission risk.

While this fact is valid for any mechanical system, it is severely amplified for space activities. Furthermore, this fact is unavoidable for any mechanical part in a satellite, but especially in the Attitude and Orbit Control System (AOCS) system. Conventional satellites use in most cases traditional reaction control systems for the basic generation of inertial torque. This category mainly includes the RWs, as well as control moment gyros. Both are based on a rotating disk, which should have a high Moment of Inertia (MoI) I along its main axis of inertia, the rotation axis. These disks are mechanically supported and accelerated or decelerated by electric motors to generate internal torque or store angular momentum in the system. This is indispensable for the attitude alignment of satellites, as well as the compensation of disturbances, especially constantly occurring disturbances such as solar radiation pressure or caused by the non-uniformity of Earth's gravity field. However, these state-of-the-art mechanical RWs, like any mechanically moving system, have the problem of wear and tear and inherent friction. This mechanical component susceptibility has previously been exposed in several space missions in the past. For instance, the space missions FUSE, Dawn, and Hayabusa, as well as the Kepler space telescope, all have the trait that at least one of their reaction wheel bearings have failed [1]. Other examples include the Neil Gehrels Swift Observatory, which went into safe mode in 2022 due to a malfunction in one of its reaction wheels [2, 3]. Another indication of the seriousness of this issue is the amount of effort spent in the space sector on measuring and classifying the reliability and lifetime of components. An example of this is the European Space Agency (ESA) product assurance data source [4].

Therefore, it is a desirable objective to design systems with a minimum amount of mechanically movable parts. Utilizing ferrofluids, or liquids responsive to magnetic fields, is one such strategy for applications requiring simplicity and reliability, i.e., space. By controlling a ferrofluid with magnetic fields rather than actuating mechanical moving components, it is possible to minimize the number of moving elements [5–8].

This paper will describe a mechanics-less RW alternative with a high potential for future space application. In this design, ferrofluid cushions reduce the wear and tear of the system.

1.1 The FARGO Project

In 2017, the Space Agency within German Aerospace Agency (DLR) launched the first Überflieger student competition, which enabled students from Germany to submit an experiment proposal. The selected winners were allowed to

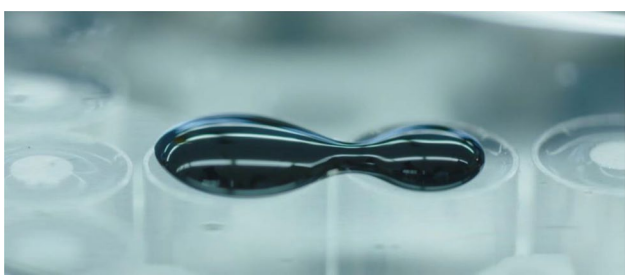

Fig. 1 Movement of a ferrofluid droplet from one electromagnet to another by an applied external magnetic field

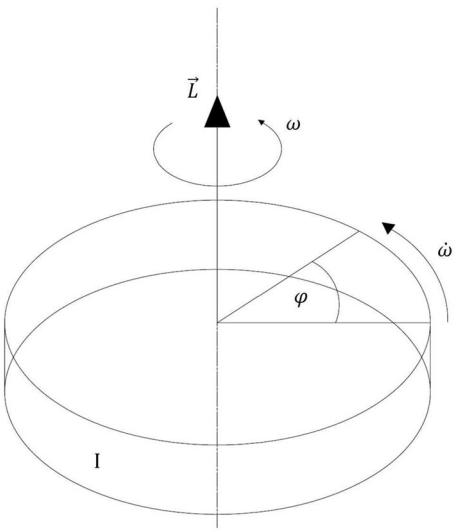

Fig. 2 Schematic illustration of a rotating rigid body

develop their experiment idea within certain project budget constraints and test it in the form of a micro-payload on the ISS. One of the winners of the first "Überflieger" project was the Small Satellite Student Society–KSat Stuttgart e.V.—with the support of the IRS with their Pump Application using Pulsed Electromagnets for Liquid reLocation (PAPELL) project. The PAPELL experiment showed a successful first proof of concept demonstration of ferrofluid manipulation in the ISS microgravity environment for future space applications. However, the manipulations were limited to simple droplet fluid movements without direct applications as an alternative component [5–8]. As a direct successor, the Überflieger 2 competition was initiated by the DLR and the Luxembourg Space Agency in late 2020 with Yuri GmbH, SpaceTango, and the DPG (German Physical Society) as co-organizers and technical advisors. For this competition, KSat e.V. submitted the FARGO project idea, which was selected as the winning proposal alongside 3 other teams. The winners will have the opportunity to realize their experiments in the form of a micro-payload of $20 \times 10 \times 10\,\mathrm{cm}^3$ with a project budget of 20 000 €. The experiments will be operated in the microgravity environment of the ISS for at least 30 days in March 2023. The experiments must be largely autonomous and are operated without the intervention of astronauts [9]. The FARGO project developed and tested three different proof of concepts for mechanically-reduced technologies with high potential in application for future spaceflight in the microgravity environment of the ISS [10–13].

This paper will focus on the Attitude Control System (ACS) experiment, which is called *Ferrowheel* as it is based on a stator of a brushless DC motor combined with a rotor on a ferrofluid bearing. Hence, the development of this ferrofluid concept from the basic idea and Earth-ground proof of concept to the design and integration of a final working prototype for in-space verification will be described.

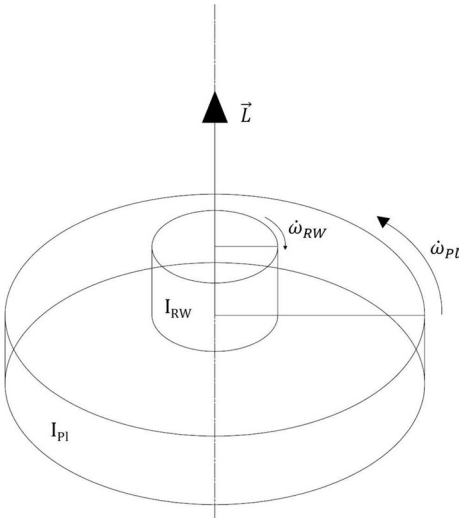

Fig. 3 Schematic illustration of a system of two rotating rigid bodies. These resemble a rotational actuator ($_{RW}$) and rotating platform ($_{Pl}$). The angular accelerations and thus the corresponding torques acting on the bodies in this system are indicated

2 Theoretical Background

In this section, a brief background on ferrofluid actuation and its relation to classic and satellite kinematics will be given.

2.1 Ferrofluid Movement

Designing low-wear systems is made possible by removing mechanical connections, which can be replaced by ferrofluid-based systems.

Ferrofluids are a suspension of paramagnetic nanoparticles of a size less than 10 nm inside a carrier fluid, in most cases oil. Within this study, EFH-1 from the Ferrotec EFH Series was chosen due to its chemical stability, low viscosity, and high magnetizability [14]. The nanoparticles experience a strong form of paramagnetism. Their very high magnetic susceptibility allows them to be rapidly magnetized by an external magnetic field. The paramagnetic particles are moving freely inside the fluid as long as no external magnetic field is applied. However, paramagnets are always attracted to the strongest point in a magnetic field, so the particles will be uniformly magnetized when an external magnetic field is applied. If a sufficiently strong external magnetic field is applied, these particles align in accordance with the magnetic field lines, thus creating the macroscopic visible magnetic reaction of ferrofluid, as shown in Fig. 1 [11, 15, 16]. A time-varying magnetic field must be applied to the ferrofluid to utilize this motion.

In this work, a stator coil of a Brushless Direct Current (BLDC) motor is used for this purpose. An outrunner BLDC motor consists of an inner stator coil segment and an outer rotating part resembling a ring of permanent magnets. The stator coils generate a time-varying, rotating magnetic field by applying an alternating 3-phase current. Thus, the outer part starts to rotate—the rotor. Such COTS stator coils are used in this work as the basis for moving ferrofluid-bearing systems through an alternating magnetic field.

2.2 Rigid-Body Rotational Motion

Considering the rotational movement of a frictionless rigid body, one sees that the angle ϕ is decisive for the definition of the angular position with respect to the chosen coordinate system, as visualized in Fig. 2. For this description, the center of mass and center of rotation are assumed to be aligned. In such a system, the angular momentum L can be defined as the product of the angular velocity ω and the MoI along the rotational axis I, while, respectively, the torque can be defined as the product of the angular acceleration $\dot{\omega}$ of the rigid body and the moment of inertia I [17, 18]

$$L = I \cdot \omega, \tag{1}$$

$$T = I \cdot \alpha = I \cdot \dot{\omega}. \tag{2}$$

For a mass point m moving with a momentum $p = mv$ at a distance r around an axis of rotation, the angular momentum L is the cross product of momentum and distance r and is thus perpendicular

$$L = p \times r. \tag{3}$$

A rotational actuator, which can be assumed as a rigid body, is depicted in Fig. 2. Under the simplifying assumption of frictionless uniformly accelerated rotational motion, the kinematic equations of the rotational motion of a rigid body about a fixed axis can be formulated in dependence on time t

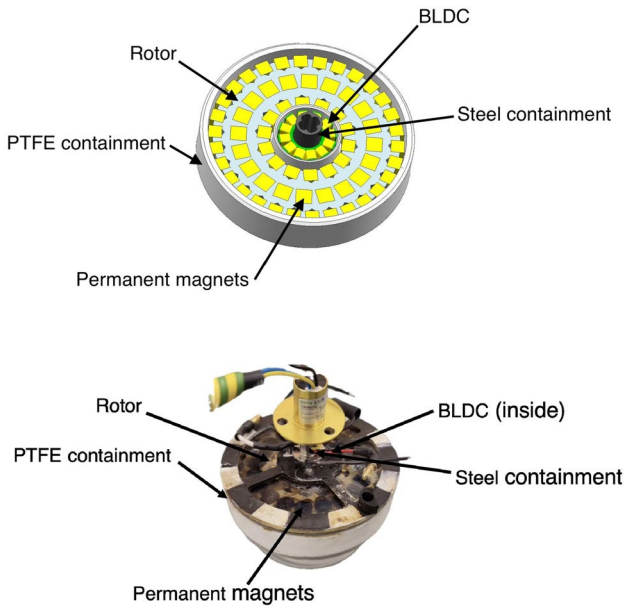

Fig. 4 Design of the Ferrowheel. Above the CAD of the system without cover, below the flight-ready Ferrowheel prototype with viewing windows

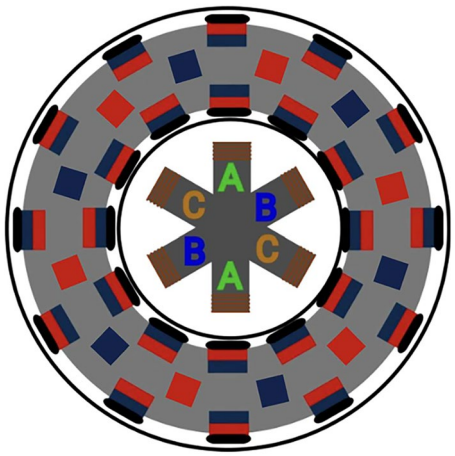

Fig. 5 Polarity and direction of the permanent magnets in the rotor. North pole in red and south pole in blue

$$\phi = \frac{1}{2}\dot{\omega}t^2 + \omega_0 t + \phi_0, \tag{4}$$

$$\omega = \dot{\omega}t + \omega_0, \tag{5}$$

$$\dot{\omega} = \alpha = \text{const.} \tag{6}$$

These equations allow the consideration of a single RW. However, if a system of RW and another rotating rigid body is considered, as visualized in Fig. 3, further interrelationships arise. This additional body could, for example, be a satellite in space or a low-friction platform. This can be assumed as a closed system of two bodies. The environment will affect this system with some amount of friction as well as the interaction between the two bodies. While these frictions can be neglected as long as they are very small, they are still noted here in the form of friction losses T_μ and L_μ, respectively

$$T_{pl} = -T_{RW} + T_\mu, \tag{7}$$

$$I_{pl} \cdot \dot{\omega}_{pl} = -I_{RW} \cdot \dot{\omega}_{RW} + T_\mu, \tag{8}$$

and

$$L_{pl} = -L_{RW} + L_\mu, \tag{9}$$

$$I_{pl} \cdot \omega_{pl} = -I_{RW} \cdot \omega_{RW} + L_\mu. \tag{10}$$

2.3 Satellite Kinematics

This rigid body rotation kinematics can be used to describe the attitude control of a satellite with an applied internal

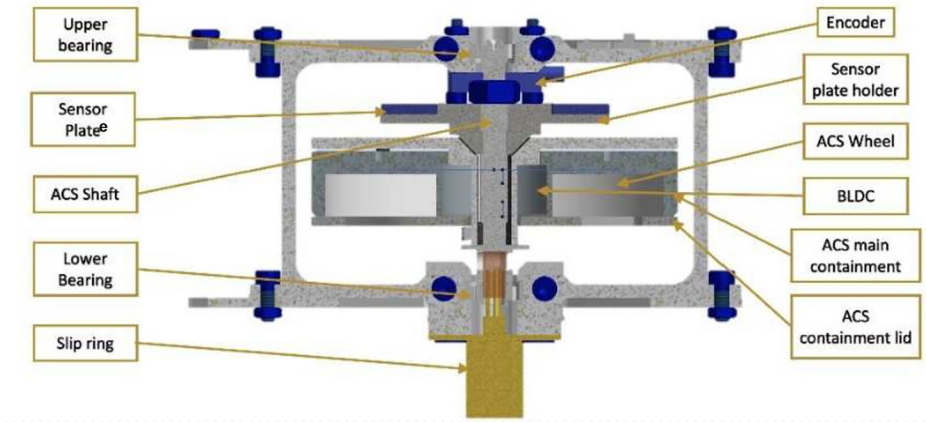

Fig. 6 CAD of the Ferrowheel integrated into the FARGO experiment. The encoder instrumentation is shown. The ACS wheel is in relative motion to the ACS main containment and is supported by the ferrofluid cushion bearing. The ACS containment is in relative motion to the main frame of the system and supported by the upper and lower mechanical bearings

torque. The attitude control with internal moments in a satellite is based on the law of conservation of angular momentum, which states that the angular momentum of a closed system remains constant as long as no external torque sources act on it. Accordingly, an RW as an internal torque source does not change the angular momentum of a satellite but only stores the angular momentum depending on its I and the speed ω until saturation at the maximum achievable speed ω_{max}.

This conservation quality of angular momentum is used in satellites for attitude control. For this purpose, the RW in a spacecraft is accelerated, whereby an angular momentum vector is formed perpendicular to the plane of rotation. Due to the conservation of angular momentum, a second angular momentum vector with the same magnitude but in the opposite direction is formed. This opposite angular momentum is responsible for the rotation of the satellite. Consequently, the satellite rotates in the opposite direction than the RW as visualized in Fig. 3 [19–22].

In the Ferrowheel experiment, this condition is simulated in a 1-axis rotation system. Instead of a complete spacecraft, a containment is introduced as a rotation platform, in which the rotor of the Ferrowheel is integrated and can perform a rotational movement, which triggers an opposite rotational reaction in the platform itself. The rotation is detected by an optical encoder, which determines the angular position.

3 General System Design Requirements

To test the concept of the Ferrowheel and to compare it with a conventional ACS, technical requirements were defined, based on the requirements for a conventional ACS:

- The Ferrowheel shall be able to generate a rotating magnetic field.
- The Ferrowheel shall be able to generate torque up to 100 mNm as the rotor and ferrofluid follow the rotation of the magnetic field of the stator.
- It shall be possible to measure the torque of the Ferrowheel.
- The Ferrowheel shall be able to generate a rotational velocity of up to 20,000 RPM [23].
- The rotation speed of the Ferrowheel shall be incrementally controllable.
- The Ferrowheel shall be able to move in a clockwise and counterclockwise direction.
- It shall be possible to measure the temperature of the Ferrowheel.
- The containment of the Ferrowheel shall be able to compensate the thermal loads.
- The Ferrowheel shall consume less energy than a conventional ACS.
- The Ferrowheel shall have a longer lifetime than a conventional ACS.
- The Ferrowheel shall achieve the same efficiency as a conventional ACS.

A desirable target for rotation speed would be at least 5000 RPM. A lifetime of up to 5 years and a power consumption less than 3 W are also desirable performance goals. These are the key data at which conventional ACS systems of similar size operate [23].

4 Ferrowheel System Design

Figure 4 shows the design of the Ferrowheel. The Ferrowheel consists of a containment structure, a stator (BLDC), a polycarbonate cover with aluminum struts, and a steel rotor. The steel rotor has a diameter of 70 mm and is covered with permanent magnets on the outside, in the center,

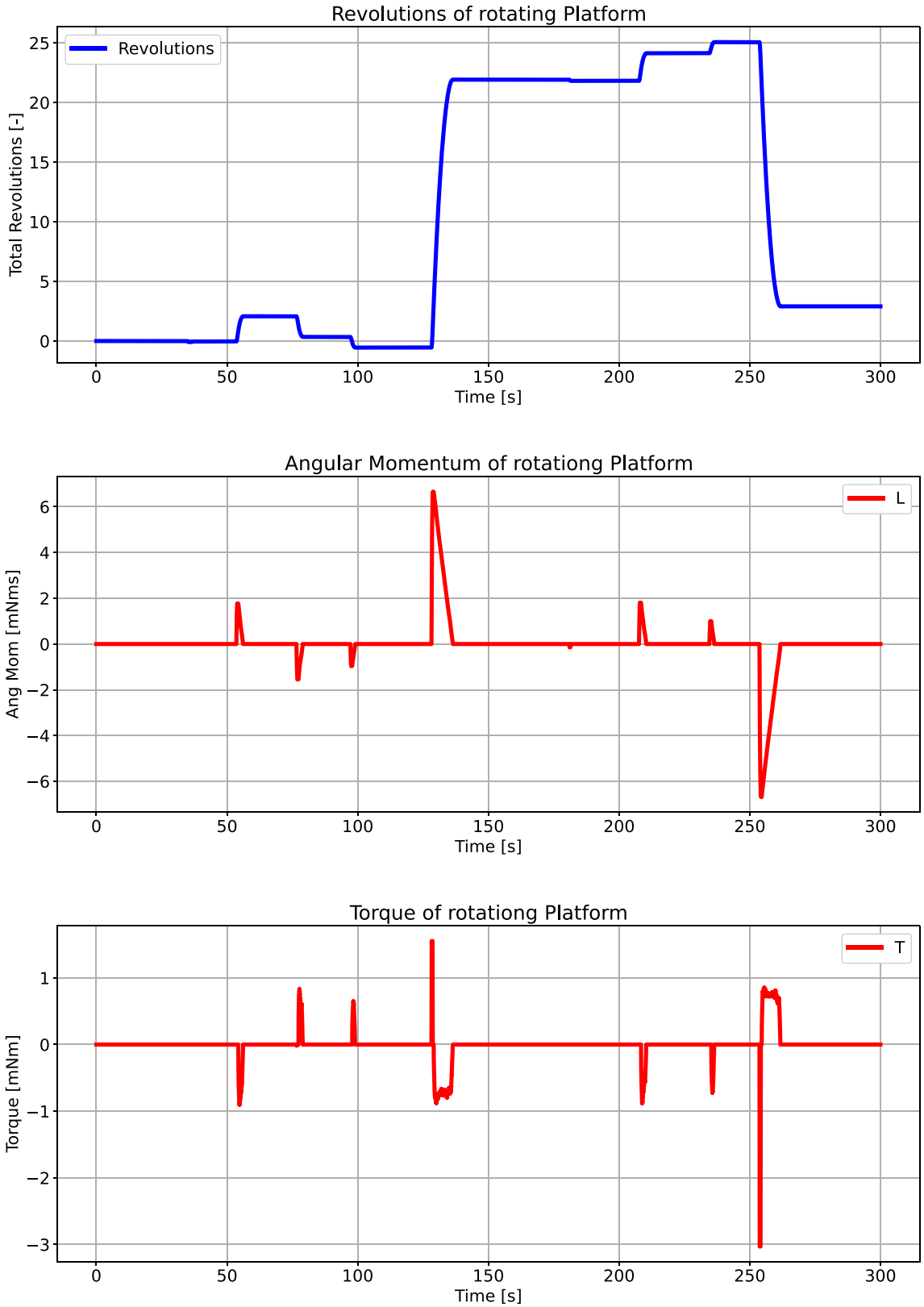

Fig. 7 From top to bottom: data from the encoder and determined angular momentum and torque

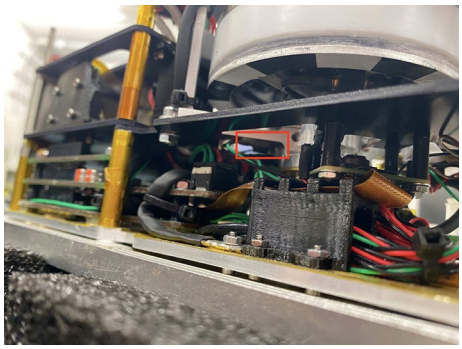

Fig. 8 Position of the internal temperature sensor on the Ferrowheel frame (red box)

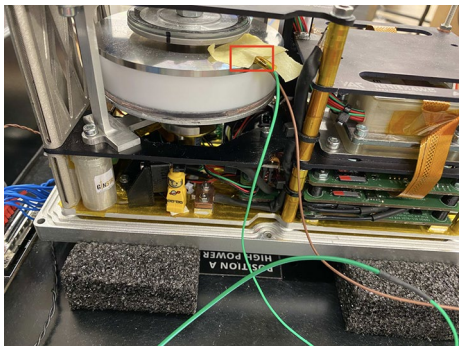

Fig. 9 Position of the PT100 temperature sensor during the long-term test (red box)

Fig. 10 Closed cube to create convective conditions as similar as possible to those on the ISS

and on the inside. The cut-out dimensions for the permanent magnets on the inside and outside are chosen, so that the magnets protrude slightly beyond the rotor structure geometry. The permanent magnets are arranged with alternating north–south polarity, so that the far magnetic field is practically zero and is focused near the surface.

Figure 5 shows the direction of the polarity of the permanent magnets and their arrangement. The poles of the inner and outer permanent magnets point perpendicular to the rotation vector. The poles of the center permanent magnet point parallel to the rotation vector. Due to this arrangement, the rotor is borne in the plane of rotation by the inner and outer permanent magnets and outside the plane of rotation by the center permanent magnets. The inner magnets also generate the torque in combination with the BLDC. The containment consists of two parts and has an outer diameter of 80 mm and a height of 16.3 mm. The main structure of the containment is made of milled PTFE (Polytetrafluoroethylene) and has an outer chamber for the rotor with ferrofluid and secondary fluid, an alcoholic fluid for air displacement, and an inner chamber for the BLDC. The paramagnetic ferrofluid adheres to the permanent magnets of the rotor and thus creates a ferrofluid cushion, which reduces wear and tear due to the fluid properties of the ferrofluid and remains positioned on the magnets due to the paramagnetic properties. The inner diameter of the inner chamber is 23 mm. The second part consists of a steel plate with an axis interface for the BLDC and is glued to the PTFE. The steel plate increases the moment of inertia and the heat dissipation into the frame structure of the FARGO experiment.

The integration is performed by wetting the permanent magnets of the rotor with ferrofluid and placing the rotor in the outer chamber of the containment. This is then filled with a secondary fluid, closed with the PC (Polycarbonate) lid, and sealed with superglue. The BLDC is glued to the aluminum struts and inserted into the inner chamber via the axis interface in the containment. The aluminum struts are glued to the PC lid and the connectors for the BLDC are attached.

For integration into the FARGO experiment, the Ferrowheel is attached to the ACS shaft with the axis interface running through the center of the containment. This setup is shown in Fig. 6. The shaft is supported by two mechanical bearings, and inserted into the precision frame. The fully assembled precision frame with integrated Ferrowheel will be mounted to the main structural plates at the top and bottom.

The Ferrowheel is controlled by a sensorless field-oriented control algorithm running on a commercial Electronic Speed Controller (ESC) board with firmware for a standard BLDC motor. An optical encoder is used to determine the torque generated. For this purpose, the sensor disk is mounted on the steel plate of the containment as shown in Fig. 6. The sensor head is located on the precision frame. In addition, a camera is mounted on the lower structural plate, which looks into the Ferrowheel, as well as an IR (infrared) sensor opposite the camera, which serves as a backup.

By changing the speed of the rotor, the containment rotates. This rotation is detected by the optical encoder and returned counts with a time stamp as angular position. The first and second derivatives give the angular velocity and the angular acceleration. From these values, the angular momentum and torque can be determined using Eqs. 1 and 2.

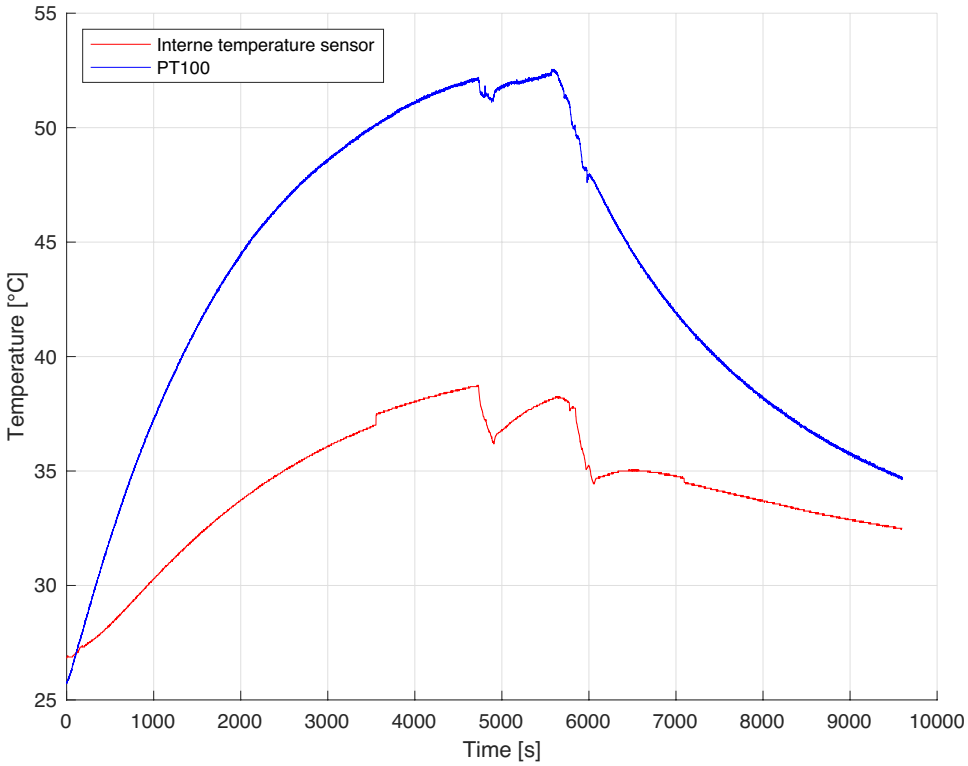

Fig. 11 Temperature curve of the internal temperature sensor and the PT100 during the long-term test at 800 RPM

5 Testing

To investigate the functionality of the Ferrowheel, various tests were performed in preparation for the FARGO experiment. In the fundamental test, the basic function was tested. For this, the Ferrowheel was started and the rotor was accelerated to 800 RPM. Afterwards, target speed was changed to 500 RPM, 300 RPM, 1000 RPM and 1200 RPM. This test was used to prove the operation capability of the system. At the same time, all sensors attached to the FARGO experiment for monitoring were tested.

Figure 7 shows the encoder output. From this, the rotation rate torque and angular momentum of the containment were determined. For the given rotor velocity changes, the maximum velocity of the containment was 30 RPM. The maximum value for the angular momentum was over 6 mNms and the generated torque was 1.8 mNm.

A second fundamental test was performed to determine an operational range for the Ferrowheel. For stable operation, the minimum rotor rotation rate was 60 RPM on the ground. To determine the maximum rotation rate of the rotor, a maximum power supply current of 1.4 A was specified for thermal reasons, with which the Ferrowheel can be operated non-destructively for a short time. Under this condition, a maximum rotation rate of 1300 RPM was achieved on the ground. The operating range of 60–1300 RPM can, most likely, be extended in space.

To investigate the performance over a longer period, a long-term test was performed at 800 RPM, during which temperature, rotation rate, and phase current were monitored. Figure 8 shows the built-in temperature sensor on the frame of the Ferrowheel.

In addition, a PT100 was placed on the containment of the ACS as shown in Fig. 9.

To create convective conditions as similar as possible to those on the ISS, the cube was sealed as shown in Fig. 10, which reduces direct large-scale convection.

The duration of the experiment was 160 min. Due to the thermal stability of PTFE, the temperature limit of the PT100 is set to 80 °C. Figure 11 shows the results of the temperature measurement.

The temperature of the PT100 increases sharply at the beginning than the temperature sensor on the frame. As can be seen in Fig. 9, the PT100 is located directly on the steel plate of the containment, which is also directly connected to the BLDC, i.e., the heat source. The temperature sensor on the frame is distanced from the BLDC. For this reason, the temperature at the sensor on the frame is lower. The temperature drop during the 90 min operation time results from the opening of the cube during the experiment for measurements via a thermal camera. It can be seen in Fig. 11 that the temperatures converge toward a constant value over time, i.e., thermal equilibrium. For a constant rotation rate of 800 RPM, the temperature of the PT100 converges toward 55 °C

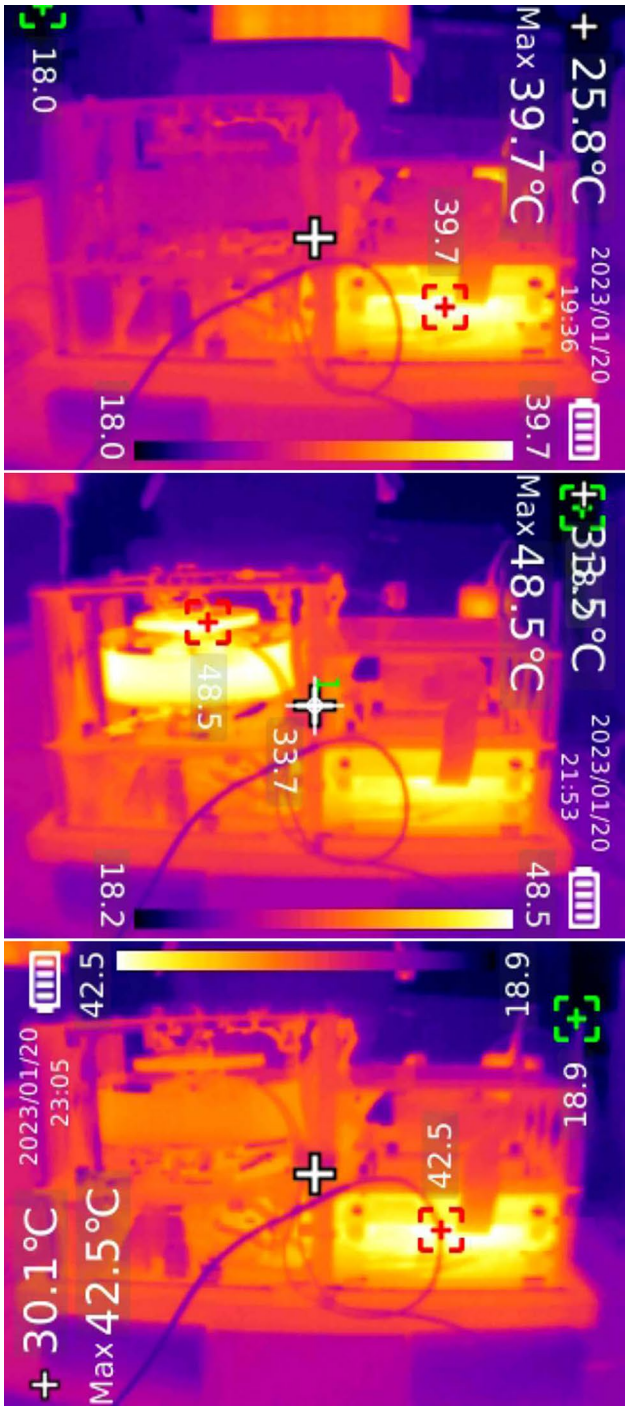

Fig. 12 Thermal image of the Ferrowheel during the long-term test. From top to bottom: before the test, after 90 min, and after 160 min

and the temperature of the sensor on the frame toward 40 °C. These temperatures are far from the limit of 80 °C. When the Ferrowheel is switched off after 90 min, the temperature drops quickly within 30 min. The heat is dissipated via the steel axis into the frame and the cube. Figure 12 shows the thermal image at the start, after 90 min and after 160 min.

In the beginning, the frame and the Ferrowheel are still at ambient temperature and only the electronics are heating up. After 90 min, the heating of the Ferrowheel and the frame is visible on the thermal image. After 160 min, the Ferrowheel has cooled significantly, and the heat has largely dissipated into the frame. For the experiment itself, the temperature sensor on the frame can be used to monitor the Ferrowheel.

To observe changes in performance over time, the rotation rate and phase current were measured and plotted in Fig. 13.

As can be seen in Fig. 13, the rotation rate is constant over 90 min and is stably controlled by the system around 800 RPM. The phase current changes more during operation, depending on the current required by the BLDC in combination with the ESC to keep the rotation rate of the rotor constant. Thus, the phase current alternates strongly. It is noticeable that the phase current drops approximately 1 A after 10 min at a constant rotation rate. A reason for this observation may be the heating of the stator. The hot stator also heats the rotor and the ferrofluid, which reduces the viscosity of the ferrofluid. As a result, less power is needed to turn the rotor, since warm ferrofluid is less viscous. For this reason, the current consumption drops to 81 % of the initial current consumption when the ferrofluid heats up. The initial power of the system is 6.48 W. Similar to the current, the power drops by 19 % to 5.28 W after 10 min.

6 Fulfillment of the Requirements

The Ferrowheel generates a rotating magnetic field and the rotor and ferrofluid follow the field. The Ferrowheel also generates a torque up to 3 mNm that can be measured. The rotor of the Ferrowheel can be controlled incrementally in a range between 60 RPM and 1300 RPM clockwise and counterclockwise. The desirable target of 5000 RPM was not achieved and is a target for future development. It is possible to measure the temperature of the Ferrowheel and set a limit for thermal destruction. In addition, the containment can compensate for thermal loads over a long period for lower rotational velocities and over a short period for higher rotational velocities. The required power of the Ferrowheel of over 5 W is much higher than the required power of less than 3 W of a conventional ACS. A goal of future developments would be to reduce the required power by optimizing the gap between the rotor and the stator. Due to the power gap, the Ferrowheel also does not reach the efficiency of a conventional ACS. A lifetime test has not been performed yet.

Not all requirements were accomplished yet, especially the performance targets compared to a conventional ACS.

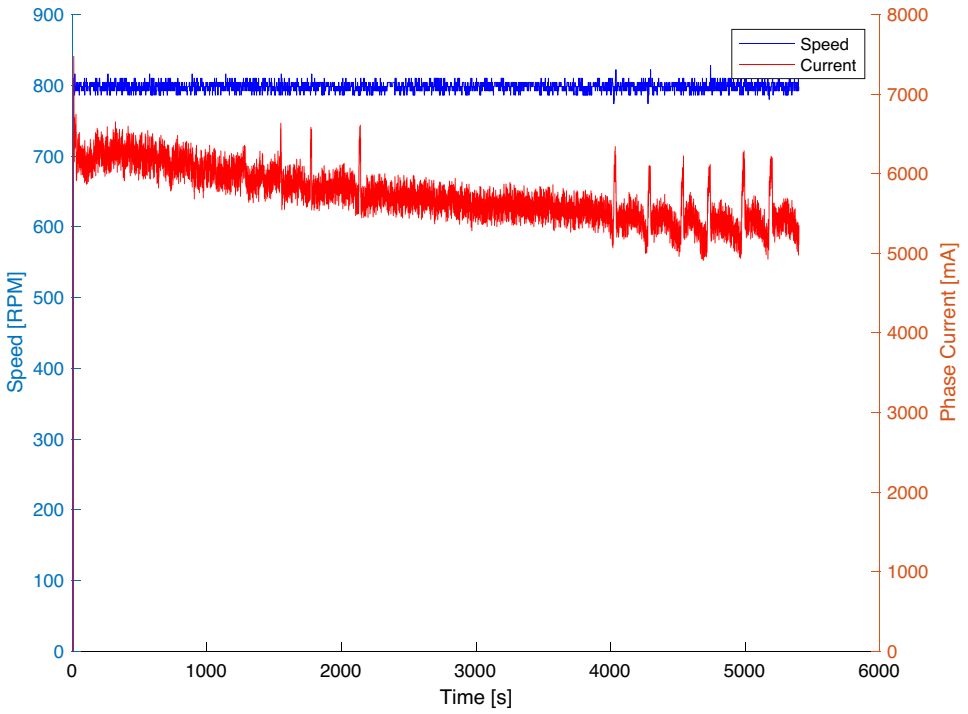

Fig. 13 Phase current and rotation rate curve during the long-term test of the Ferrowheel at 800 RPM

However, the Ferrowheel fulfilled all basic requirements and reached a high level in the short development time of a single year.

7 Conclusion

In the research discussed here, a working prototype of a novel RW based on a ferrofluid bearing rather than a mechanical bearing was presented. The Ferrowheel was explained from its concept study, through development to final design and integration. In addition, preliminary verifying tests were detailed. The design-critical points of the system were highlighted and the general functionality on the ground was shown. Furthermore, this research shows that ferrofluid-based RWs have the potential to replace conventional RWs in the future.

The COTS BLDC has turned out to be a critical point of the development, as both the control is not trivial and the part is fragile when manually produced and therefore tends to fail during integration, which has usually led to a complete replacement of the BLDC. In addition, it became apparent that such a rotating system requires precise manufacturing on the order of hundreds µm, especially in the area of the rotor, to avoid residual friction or grinding and therefore wear and tear. The temperature development of the BLDC, especially at high speeds, turns out to be a main design driver, as temperature is a very critical point to avoid components overheating or melting. Therefore, further design for heat mitigation and cooling systems should be considered. As a further point, the potential for reducing the system mass compared to conventional RWs should be investigated, as such a mass reduction could be possible with this concept and would be highly beneficial for space missions.

In conclusion, the system discussed here cannot yet keep up with conventional RW systems but is on a promising path toward competitiveness. If one compares the decades of heritage of conventional systems with the development time that has elapsed so far for ferrofluid systems, it becomes clear that these systems have already reached a considerable level in a very short time, within a student project and that future potential is apparent.

Both short-term high rotation rates of over 1000 RPM and long-term operation of almost 2 h at lower rotation rate ranges were already possible with the system. Even longer operating periods are also possible but are subject to future testing. Thus, this paper represents the entire development of the system up to the integration into the FARGO cube for implementation on the ISS. The Ferrowheel was successfully put into operation on the ISS in March 2023. The basic functionality of the system was thus demonstrated both on the ground and in space. The data obtained from this operation will provide an important basis for future research on this system [24].

8 Outlook

The work on ferrofluid as a competitive technology for mechanical RWs is very promising and offers great potential for the future of space activities. Therefore, building on this work, research on the Ferrowheel will continue in the future in the cooperation between KSat e.V. and IRS. Further research and development work may lead to the Ferrowheel replacing a conventional ACS in spacecraft.

As already mentioned, current issues include optimizing the precision of the production of all components, in particular the rotor, and implementing a cooling system to avoid high temperatures. In addition, the electric control of the BLDC should be optimized for usability, range and reliability.

The next big step for the Ferrowheel experiment after this development was the operation on board of the ISS for 30 days in March 2023. This provided in-space verification of the system, and the resulting data will be of significant value for the further development of the system [24].

Acknowledgements The FARGO project as well as the Ferrowheel experiment is made possible by support from the space agency within DLR as part of the Überflieger 2 competition. The authors would like to thank the DLR, DPG, Yuri GmbH, SpaceTango, and all other supporters contributing to this research. In addition, the authors would like to thank the IRS for sharing their academic expertise. Last but not least, the authors would like to thank our association KSat e.V. for providing the necessary laboratory and our FARGO team for their dedication and hard work toward the realization of this project.

Funding Open Access funding enabled and organized by Projekt DEAL.

Data availability The data are available. The release of the data must be decided by the KSat. e.V.

Declarations

Conflict of Interest On behalf of all authors, the corresponding author states that there is no conflict of interest.

References

1. AEGIS: In Space, No One Can Hear Your Bearings Fail. https://blog.est-aegis.com/in-space-no-one-can-hear-your-bearings-fail. Accessed 09 Feb 2023
2. Gohd, C.: NASA's gamma-ray observatory is in safe mode after a possible wheel failure. https://www.space.com/nasa-swift-observatory-safemode-reaction-wheel. Accessed 09 Feb 2023
3. Howell, E.: NASA's gamma-ray observatory is back in action after technical glitch. https://www.space.com/nasa-gamma-rayobservatory-back. Accessed 09 Feb 2023
4. ESA: ECSS-Q-HB-30-08A. Space product assurance (2021)
5. Ehresmann M., Hild F., et al.: PAPELL: Solid-state pumping mechanism: Presented at Human Spaceflight and Weightlessness Science, Toulouse (2018)
6. Ehresmann M., Hild F., et al.: PAPELL: Mechanic-free Actuators through Ferrofluids: Presented at 12th IAA Symposium on Small Satellites for Earth Observation, Berlin (2019)
7. Hild F., Grundwald K., et al.: PAPELL: Final Student Experiment Design of a Non-mechanical Pumping System on the ISS: Presented at 69th International Astronautical Congress IAC, Bremen (2018)
8. Sütterlin, S., Bölke, D., et al.: FARGO-Validation of space-relevant ferrofluid applications on the ISS; Presented at 71st DLRK Symposium, Dresden (2022)
9. DLR: Studierendenwettbewerb Überflieger 2: Experimente für die ISS. https://www.dlr.de/rd/desktopdefault.aspx/tabid11751/20568_read-48090/. Accessed 09 Feb 2023
10. KSat-e.V.: Ferrofluid Application Research Goes Orbital. https://www.ksatstuttgart.de/de/fargo. Accessed 09 Feb 2023
11. Breitenbücher, L.: Assessment of Ferrofluid interaction with secondary liquids; Bachelor Thesis, Institute of Space Systems, University of Stuttgart (2020)
12. NASA: Überflieger 2: Ferrofluid Application Research Goes Orbital. https://www.nasa.gov/mission_pages/station/research/experiments/explorer/Investigation.html?#id=8949. Accessed 09 Feb 2023
13. Heinz N., Ehresmann M., et al.: The Student Project FARGO - A Ferrofluid Experiment on the ISS: Presented at the 74th International Astronautical Congress (IAC), Baku (2023)
14. GmbH, F.: Safety data sheet EFH-1. https://ferrofluid.ferrotec.com/wp-content/uploads/sites/3/efhsds.pdf. Accessed 09 Feb 2023
15. Odenbach, S.: Ferrofluids: Magnetically Controllable Fluids and Their Applications. Springer, Berlin (2002)
16. Papell, S. S., Faber, C. O.: On the Influence of nonuniform Magnetic Fields on FerromagneticnColloidal Sols; NASA Technical Note TN D-4676, Lewis Research Center Cleveland, Ohio. https://ntrs.nasa.gov/api/citations/19680020572/downloads/19680020572.pdf. Accessed 09 Feb 2023
17. Demtroeder, W.: Mechanics and Thermodynamics - Undergraduate Lecture Notes in Physics. Springer, Kaiserslautern (2017). (**ISBN: 978-3-319-27875-9**)
18. Karaoglu, B., Karaoglu, M.: Classical Physics: A Two-Semester Coursebook. Springer, Istanbul (2020). (**ISBN: 978-3-030-38455-5**)
19. Sidi, M.J.: Spacecraft Dynamics and Control: A Practical Engineering Approach. Cambridge Univ Press, Cambridge (1997). (**ISBN:0-521-55072-6**)

20. Leve, F.A., Hamilton, B.J., Peck, M.A.: Spacecraft Momentum Control Systems. Springer, Cham (2015). (**ISBN: 978-3-319-22562-3**)
21. Messerschmid, E., Fasoulas, S.: Raumfahrtsysteme - Eine Einführung Mit Übungen und Lösungen. Springer, Berlin (2017). (**ISBN: 978-3-662-49637-4**)
22. Mazzini, L.: Flexible Spacecraft Dynamics, Control and Guidance. Springer, Cham (2016). (**ISBN: 978-3-319-25538-5**)
23. Korn, C.: Design and Manufacture of a Torque Measuring Test-Bed for Experimental Attitude Control Actuators; Bachelor Thesis, Institute of Space Systems, University of Stuttgart (2020)
24. Dietrich, J., Ehresmann, M., et al.: Scientific Results of FARGO - A Verification of Novel Ferrofluid Systems on the ISS: Presented at the 74th International Astronautical Congress (IAC), Baku (2023)